J Arid Land (2025) 17(2): 182–199
doi: 10.1007/s40333-025-0090-y; CSTR: 32276.14.JAL.0250090y

Science Press Springer-Verlag

Impact of climate change and land use/cover change on water yield in the Liaohe River Basin, Northeast China

LYU Leting[1,2*], JIANG Ruifeng[1], ZHENG Defeng[1,2], LIANG Liheng[3]

[1] College of Geosciences, Liaoning Normal University, Dalian 116029, China;
[2] Dalian Key Laboratory of Agro-Meteorological Disaster Risk Prevention and Control, Dalian 116029, China;
[3] College of Geographic Sciences, Changchun Normal University, Changchun 130032, China

Abstract: The Liaohe River Basin (LRB) in Northeast China, a critical agricultural and industrial zone, has faced escalating water resource pressures in recent decades due to rapid urbanization, intensified land use changes, and climate variability. Understanding the spatiotemporal dynamics of water yield and its driving factors is essential for sustainable water resource management in this ecologically sensitive region. This study employed the Integrated Valuation of Ecosystem Services and Tradeoffs (InVEST) model to quantify the spatiotemporal patterns of water yield in the LRB (dividing into six sub-basins from east to west: East Liaohe River Basin (ELRB), Taizi River Basin (TRB), Middle Liaohe River Basin (MLRB), West Liaohe River Basin (WLRB), Xinkai River Basin (XRB), and Wulijimuren River Basin (WRB)) from 1993 to 2022, with a focus on the impacts of climate change and land use cover change (LUCC). Results revealed that the LRB had an average annual precipitation of 483.15 mm, with an average annual water yield of 247.54 mm, both showing significant upward trend over the 30-a period. Spatially, water yield demonstrated significant heterogeneity, with higher values in southeastern sub-basins and lower values in northwestern sub-basins. The TRB exhibited the highest water yield due to abundant precipitation and favorable topography, while the WRB recorded the lowest water yield owing to arid conditions and sparse vegetation. Precipitation played a significant role in shaping the annual fluctuations and total volume of water yield, with its variability exerting substantially greater impacts than actual evapotranspiration (AET) and LUCC. However, LUCC, particularly cultivated land expansion and grassland reduction, significantly reshaped the spatial distribution of water yield by modifying surface runoff and infiltration patterns. This study provides critical insights into the spatiotemporal dynamics of water yield in the LRB, emphasizing the synergistic effects of climate change and land use change, which are pivotal for optimizing water resource management and advancing regional ecological conservation.

Keywords: Liaohe River Basin; water yield; Integrated Valuation of Ecosystem Services and Tradeoffs (InVEST) model; climate change; land use cover change (LUCC)

Citation: LYU Leting, JIANG Ruifeng, ZHENG Defeng, LIANG Liheng. 2025. Impact of climate change and land use/ cover change on water yield in the Liaohe River Basin, Northeast China. Journal of Arid Land, 17(2): 182–199. https://doi.org/10.1007/s40333-025-0090-y; https://cstr.cn/32276.14.JAL.0250090y

1 Introduction

Ecosystems provide diverse services, including provisioning, regulating, cultural, and supporting functions; among these, water resources are of paramount importance for maintaining both ecological balance and human well-being (Li et al., 2024a). Water resources are critical to

*Corresponding author: LYU Leting (E-mail: lvleting@lnnu.edu.cn)
Received 2024-07-25; revised 2024-11-23; accepted 2024-11-28

sustaining agricultural and industrial development, meeting human consumption needs, and supporting diverse aspects of daily life. The global demand for water resources is rising steadily, driven by population growth, economic expansion, and increasing standards of living. In China, this trend is particularly pronounced due to the high demand for food production and significant regional development imbalances, which have intensified pressures on water resource utilization and equitable distribution (Song et al., 2024). China possesses only 6.00% of the world's freshwater resources and faces significant challenges due to substantial north-south disparities, leading to pronounced water resource scarcity issues (Wang et al., 2022a). Against this backdrop, water yield, as a key metric for evaluating water supply capacity and ecosystem functionality, has garnered increasing attention. Quantitative assessment and visualization of water yield are essential for understanding trends and drivers of ecosystem water-supply functions while also shedding light on the significant impacts of human activities on water resources. These evaluations enable scientists to identify and forecast changes in ecosystem functions, offering a scientific foundation for conserving and equitably distributing water resources, thereby supporting the sustainable development of ecosystem services.

Climate change has a significant impact on water yield. For example, global warming alters evapotranspiration and precipitation patterns, which directly affect the availability and distribution of water resources (Li et al., 2024b). Changes in land use, such as deforestation, agricultural expansion, and urbanization, can modify the landscape's capacity to retain and regulate water, further influencing water yield (Rodríguez and Mazza, 2020). These alterations in water availability and distribution also have profound effects on ecosystem functions, such as soil conservation, biodiversity preservation, and climate regulation. The combined impacts of climate change and land use change have led to a progressive deterioration of ecological environment, as altered water cycles disrupt vital ecosystem services and increase the vulnerability of ecosystems to environmental stress (Hasan et al., 2020; Malhi et al., 2020).

In this context, numerous tools are now available for mapping and delineating ecosystem services, as well as quantifying the impacts of environmental changes. The Integrated Valuation of Ecosystem Services and Tradeoffs (InVEST) model, collaboratively developed by Stanford University, the Nature Conservancy, and the World Wildlife Fund, incorporates a water yield module based on hydrological cycle. Supported by ArcGIS software (Esri, Redlands, California, USA), this module can quantify the water yield of all land use types within an area. The output, which represents the water yield of raster units, enables the calculation of water yield volume in the study area, thereby supporting a multi-scale, comprehensive, dynamic, and visual assessment of water ecosystem service functions. To date, the InVEST model's water yield module has been applied in various regions, such as Patuha Mountain and Tesso Nilo National Park in Indonesia (Yudistiro et al., 2019; Ningrum et al., 2022), 22 watersheds in the United Kingdom (Redhead et al., 2016), mangroves in southern Iran (Dashtbozorgi et al., 2023), and the Yellow River and Weihe River basins in China (Yin et al., 2021; Wu et al., 2022). Through water yield assessments, previous studies have quantified hydrological services and have explored the spatial distribution patterns and driving factors of water-related ecosystem services, such as water conservation, soil erosion control, and biodiversity preservation by applying hot and cold spot analysis and correlation analysis. These findings provide valuable theoretical insights and practical guidance for regional water resource management and ecological protection (Wang et al., 2022a; Guo et al., 2023). In addition, scholars have investigated the impacts of climate change and land use cover change (LUCC) on watershed water yield. For example, Nahib et al. (2021) focused on the sensitivity of water yield in the Citarum River Basin, Indonesia, to climate change and land use change, revealing that climatic parameters, mainly changes in precipitation, which have the most significant impact, followed by evapotranspiration, play a primary role in influencing water yield. Emlaei et al. (2022) analyzed the impact of LUCC on water yield in Iran's Haraz Basin, and the results showed that the transitions among cultivated land, construction land, and forest land have the most significant impact on water yield.

The Liaohe River Basin (LRB) is a water-scarce region in China, particularly in its middle and lower reaches, where water resources are under significant pressure due to high population density as well as agricultural and industrial development (Zheng, 2018). The forests, widely distributed across the basin, play a crucial role in maintaining soil and water quality; however, the degradation of these forests, driven by various human activities, threatens the sustainable use of water resources (Yang, 2024). Furthermore, climate change has exacerbated the vulnerability of water resources in this region, with water yield becoming a key factor limiting the sustainable development of both society and economy (Daneshi et al., 2021; Wang et al., 2022b). Current research on the LRB mainly focused on regional ecological security models (Mao et al., 2020), relationships in ecosystem services (Zhang et al., 2021a), and the effects of meteorological factors on evapotranspiration (Jiang and Xin, 2022). Thus, the assessment of water yield influenced by climate change and land use change in the LRB is necessary. The aims of this study are to: (1) simulate water yield of the LRB from 1993 to 2022 and analyze its spatiotemporal variations; (2) use scenario analysis to quantitatively assess the impacts of climate change and land use change on water yield; and (3) discuss mechanisms for regulating water yield. The research results can provide a scientific basis for understanding the impacts of climate change and land use change on water resources in the LRB, and offer practical guidance for watershed water resource management and ecological protection.

2 Materials and methods

2.1 Study area

The LRB is located in Northeast China, belonging to the ecological transition zone between the Mongolian Plateau and the North China Plain (40°30′15″–45°10′45″N, 116°30′30″–125°47′15″E; Fig. 1). As one of the largest water systems of China, the LRB flows through Liaoning Province, Jilin Province, Hebei Province, and Inner Mongolia Autonomous Region. The LRB is composed of six major sub-basins, which, from east to west, are the East Liaohe River Basin (ELRB), Taizi River Basin (TRB), Middle Liaohe River Basin (MLRB), West Liaohe River Basin (WLRB), Xinkai River Basin (XRB), and Wulijimuren River Basin (WRB), encompassing a total area of 21.46×10^4 km^2. The topography is characterized by mountains and plains, with mountains locating on the east and west sides of the basin and the central part consisting of the Liaohe River alluvial plain, which is generally high in the west and low in the east. The region experiences a temperate to cold-temperate continental monsoon climate, with an average annual temperature of approximately 5°C. The lowest temperatures typically occur in January, averaging around –10°C, while the highest temperatures usually occur in July, averaging around 30°C. Precipitation and runoff are unevenly distributed throughout the year (Zheng, 2018). The dominated land use types within the LRB are cultivated land and grassland, accounting for 37.88% and 28.93% of the total area, respectively.

2.2 Data sources and processing

The data employed in this study included Digital elevation model (DEM), climate (including precipitation, temperature, and solar radiation), land use/land cover (LULC), and soil data (sand, silt, and clay contents and organic carbon content). Utilizing the ArcGIS v.10.8 software, we divided the LRB into six sub-basins through iterative hydrological connectivity analysis and watershed threshold optimization based on DEM data: ELRB, TRB, MLRB, WLRB, XRB, and WRB. The LULC data were reclassified into six types: cultivated land, forest land, grassland, water body, construction land, and unused land. Meteorological data were derived from 21 meteorological stations surrounding the LRB (Fig. 1), covering observational records from 1993 to 2022, and were spatially interpolated using the Kriging method to generate raster datasets. Detailed data sources are presented in Table 1.

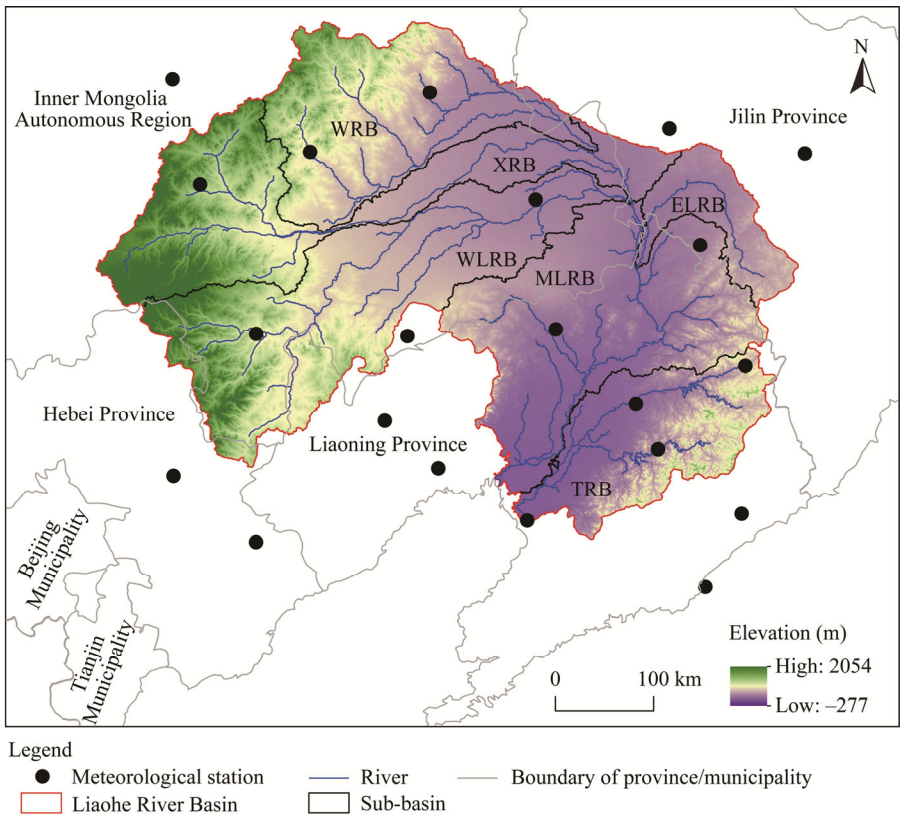

Fig. 1 Overview of the Liaohe River Basin (LRB), China. WLRB, West Liaohe River Basin; WRB, Wulijimuren River Basin; XRB, Xinkai River Basin; MLRB, Middle Liaohe River Basin; ELRB, East Liaohe River Basin; TRB, Taizi River Basin.

Table 1 Relevant basic data sources

Data	Indicator	Resolution	Year	Data source
Terrain data	Digital elevation model (DEM, m)	30 m	2020	Geospatial Data Cloud Platform, Chinese Academy of Sciences (https://www.gscloud.cn/)
Climate data	Daily precipitation (mm)	1 km	1993–2022	China National Meteorological Information Center (https://data.cma.cn/)
	Daily maximum temperature (°C)			
	Daily minimum temperature (°C)			
	Solar radiation (MJ/(m^2•d))			Food and Agriculture Organization of the United Nations (https://www.fao.org/home/zh)
Land use data	Land use/land cover (LULC)	30 m	1995, 2000, 2005, 2008, 2010, 2015, 2018, and 2020	Resource and Environmental Science Data Center, Chinese Academy of Sciences (http://www.resdc.cn)
Soil data	Soil texture	1 km	2009	Harmonized World Soil Database (http://iiasa.ac.at/models-tools-data/hwsd)
	Soil organic carbon (%)	1 km	2009	National Tibetan Plateau Data Center https://data.tpdc.ac.cn
	Soil depth (mm)	1 km	2016	International Soil Reference and Information Centre https://www.isric.org

Note: Soil texture represents the contents of clay, sand, and silt in the soil (%); soil depth refers to the maximum depth to which plant roots can extend in the soil, influenced by the physical and chemical characteristics of the environment.

2.3 InVEST model

2.3.1 Water yield and water yield rate

The InVEST water yield module, grounded in the Budyko's hypothesis of coupled water-energy balance, employs a modeling framework to quantify hydrological processes (Qi et al., 2021). The approach relies on gridded spatial data to calculate water yield, where water yield within each pixel of the watershed is derived as the difference between precipitation and actual evapotranspiration (AET) (Li et al., 2021a). The InVEST model integrates key influencing factors, including soil texture and structure, precipitation characteristics, surface transpiration, land use patterns, and water resource confluence, to accurately characterize the spatial distribution and dynamic variations of watershed water resources (Li et al., 2023). The formulae are as follows:

$$Y(x)=\left(1-\frac{\mathrm{AET}(x)}{P(x)}\right)\times P(x), \tag{1}$$

$$Y_{\mathrm{vol}}(x)=\left(1-\frac{\mathrm{AET}(x)}{P(x)}\right)\times P(x)\times A(x), \tag{2}$$

where $Y(x)$ is the annual water yield of grid cell x (mm); AET(x) is the annual actual evapotranspiration of grid cell x (mm); $P(x)$ is the annual precipitation of grid cell x (mm); $Y_{\mathrm{vol}}(x)$ is the annual water yield volume of grid cell x (m^3); and $A(x)$ is the area of grid cell x (m^2).

For vegetation land, we derived AET based on Budyko's water balance curve as follows (Zhang et al., 2004; Li et al., 2022):

$$\frac{\mathrm{AET}(x)}{P(x)}=\frac{1+\omega(x)\left[\mathrm{PET}(x)/P(x)\right]}{1+\omega(x)\left[\mathrm{PET}(x)/P(x)\right]+1/\left[\mathrm{PET}(x)/P(x)\right]}, \tag{3}$$

where $\frac{\mathrm{PET}(x)}{P(x)}$ is the Budyko dryness index; $\omega(x)$ is the non-physical empirical fitting parameter of soil properties under natural climatic conditions in the catchment; and PET(x) is the potential evapotranspiration of grid cell x (mm). The formulae describing the calculation of PET (Gomariz-Castillo et al., 2018), the non-physical empirical fitting parameter (Donohue et al., 2012), and the relationship between soil properties, climate, and evapotranspiration in a given grid cell are as follows (Zhang et al., 2020):

$$\mathrm{PET}(x)=K_c(l_x)\times \mathrm{ET}_0(x), \tag{4}$$

$$\mathrm{ET}_0(x)=0.0013\times 0.408\times Ra\times\left[\left(\frac{T_{\max}+T_{\min}}{2}\right)+17\right]\times\left[\left(T_{\max}-T_{\min}\right)-0.0123P\right]^{0.76}, \tag{5}$$

$$\omega(x)=1.25+Z\frac{\mathrm{AWC}(x)}{P(x)}, \tag{6}$$

$$\mathrm{AWC}(x)=\min(\mathrm{MSD}_x,\mathrm{RD}_x)\times\mathrm{PAWC}_x, \tag{7}$$

$$\mathrm{PAWC}_x=54.509-0.132\mathrm{Sand}-0.003(\mathrm{Sand})^2-0.055\mathrm{Silt}-0.006(\mathrm{Silt})^2-0.738\mathrm{Clay}+0.007(\mathrm{Clay})^2-2.688\mathrm{OC}+0.501(\mathrm{OC})^2, \tag{8}$$

where $K_c(l_x)$ is the vegetation evapotranspiration coefficient for a specific land use type in grid cell x; and $\mathrm{ET}_0(x)$ is the reference evapotranspiration of grid cell x (mm); Ra is the solar radiation (MJ/(m^2·d)); $T_{\max}$ is the average of the daily maximum temperatures recorded throughout the year (°C); $T_{\min}$ is the average of the daily minimum temperatures recorded throughout the year (°C); P is the sum of the daily precipitation amounts recorded throughout the year (mm); AWC(x) is the effective soil water content (mm), i.e., the total amount of water that the soil can effectively store and supply for plant growth, determined by soil texture and effective soil depth; Z is the empirical constant that can effectively integrate the precipitation distribution pattern with the hydrogeological characteristics of the study area; MSD_x is the maximum soil depth (mm),

representing the total thickness of soil available before encountering a restrictive layer; RD_x is the actual root depth of vegetation (mm), which is bounded by the soil depth and plant characteristics (Table 2); $PAWC_x$ is the plant available water content of grid cell x (mm); and Sand, Silt, Clay, and OC are the contents of sand, silt, clay, and organic carbon in the soil, respectively (%). The K_c value of each land use type was referred to Li et al. (2023).

The water yield rate is an indicator of the water production capacity of different land use types in the same area, and is determined as (Kiziloglu et al., 2009):

$$\mathrm{WYR} = \frac{Y(x)}{A(x)} \times 100\%, \tag{9}$$

where WYR is the water yield rate (%).

Table 2 Biophysical coefficients for the Integrated Valuation of Ecosystem Services and Tradeoffs (InVEST) model

Land use type	K_c	LULC_veg	RD (mm)
Cultivated land	0.65	1	300
Forest land	1.00	1	3000
Grassland	0.65	1	2000
Water body	1.00	0	1
Construction land	0.30	0	1
Unused land	0.30	0	1

Note: K_c, vegetation evapotranspiration coefficient; LULC_veg, land use/land cover with vegetation cover; RD, root depth.

2.3.2 Model calibration

The water yield module of the InVEST model was utilized to simulate the natural runoff of a watershed, with its accuracy highly dependent on the parameter Z. Based on the results derived from gridded daily precipitation data within the Global Precipitation Climatology Centre (GPCC) dataset as applied by Guo et al. (2023), the Z value ranges between 15.00 and 25.00. When the Z value was set to 20.50, the average water yield volume of the LRB reached 53.13×10^9 m^3, which closely approximates the statistical estimate of 51.00×10^9 m^3 reported by Zhang (2021). Consequently, this study adopted 20.50 as the optimal Z value.

2.4 Climate scenario settings

To investigate the response of water yield to climate change, we utilized the InVEST model to simulate and evaluate their impacts. We researched the impact of climatic conditions on water yield, focusing exclusively on changes in precipitation and evapotranspiration, due to the impact temperature on water yield is mainly indirect through evapotranspiration.

Based on the classification standards of precipitation types, we classified the study period of 1993–2022 into three categories: wet year ($P_w>P+0.33\sigma$), normal year ($P-0.33\sigma<P_w<P+0.33\sigma$), and dry year ($P_w<P-0.33\sigma$), of which P_w is the annual precipitation of a specific year, P is the average annual precipitation, and σ is the standard deviation of annual precipitation (Zhang et al., 2021b). According to this method, in the study period, we identified 1993, 1994, 1995, 1998, 2005, 2010, 2012, 2013, 2016, 2018, 2019, 2020, 2021, and 2022 as wet year; 1996, 1997, 2003, 2004, 2008, 2015, and 2017 as normal year; and 1999, 2000, 2001, 2002, 2006, 2007, 2009, 2011, and 2014 as dry year.

2.5 Hotspot and coldspot analysis (Getis-Ord G_i^*)

Getis-Ord G_i^* analysis is an inferential statistical method used to detect clustering patterns in spatial data. Typically, the G_i^* statistic proposed by Getis and Ord (1995) is employed for calculation, and its statistical significance is tested using standardized $Z(G_i^*)$ (Ren et al., 2023). After significance testing, the results are expressed in terms of $Z(G_i^*)$. A positive $Z(G_i^*)$ indicates the clustering of high-value attributes (hotspot) within the study area, while a negative $Z(G_i^*)$

suggests the clustering of low-value attributes (coldspot). We further divided all basins into 126 sub-basins based on their geographic and hydrological boundaries to ensure scientific accuracy and spatial precision (Xu et al., 2015). In this study, the spatial clustering characteristics of water yield were analyzed using ArcGIS v.10.8 software, where hotspots represent areas of concentrated high water yield, and coldspots represent areas of concentrated low water yield. The specific calculation formulae are as follows (Griffith, 2021):

$$G_i^* = \frac{\sum_{j=1}^{n} W_{ij} x_j}{\sum_{j=1}^{n} x_j}, \tag{10}$$

$$Z(G_i^*) = \frac{\sum_{j=1}^{n} W_{ij} - \frac{\sum_{j=1}^{n} x_j}{n} \sum_{j=1}^{n} W_{ij}}{\sqrt{\frac{n \sum_{j=1}^{n} W_{ij}^2 - (\sum_{j=1}^{n} W_{ij})^2}{n-1}}}, \forall j \neq i, \tag{11}$$

where G_i^* is the local spatial clustering of water yield; $Z(G_i^*)$ is the standardized score of G_i^*, used to test the statistical significance of this clustering; W_{ij} is the spatial weight between sub-basin i and sub-basin j; n is the total number of sub-basins; and x_i and x_j are the water yield values of sub-basin i and sub-basin j, respectively.

3 Results

3.1 Spatiotemporal variation characteristics of water yield in the LRB

3.1.1 Temporal variation characteristics

From 1993 to 2022, the temporal variations of precipitation, AET, and water yield in the LRB exhibited distinct patterns (Fig. 2). The average annual precipitation was 483.15 mm, which showed a significant upward linear trend at a rate of 27.03 mm/10a (P<0.05), with the highest precipitation recorded in 2021 (667.00 mm) and the lowest in 2009 (353.00 mm). The AET averaged 235.60 mm and displayed a significant upward trend at a rate of 4.07 mm/10a (P<0.05), peaking at 266.20 mm in 2019 and reaching its minimum of 207.20 mm in 2000. Water yield exhibited considerable inter-annual variability, with an average of 247.54 mm and a slight but significant upward trend of 22.96 mm/10a (P<0.05). The highest water yield was recorded in 2021 (408.90 mm), while the lowest occurred in 2009 (145.10 mm). These findings indicated that the hydrological characteristics of the LRB underwent significant changes during the study period.

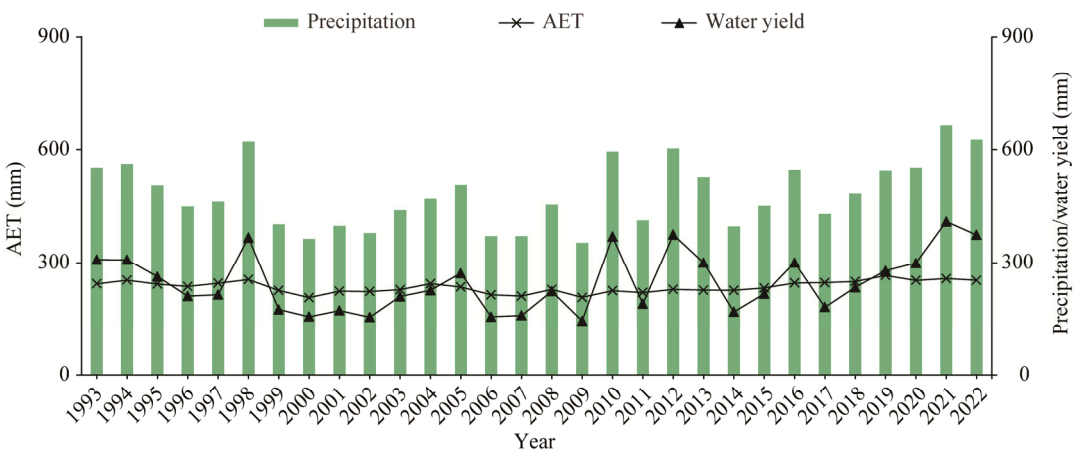

Fig. 2 Precipitation, actual evapotranspiration (AET), and water yield in the LRB from 1993 to 2022

3.1.2 Spatial variation characteristics

The LRB demonstrated significant spatial variations in precipitation, AET, and water yield across its six major sub-basins (Tables 3 and 4). The TRB exhibited the highest average annual precipitation (710.37 mm), average annual AET (275.46 mm), and average water yield rate (47.67%). Although it covered only 12.09% of the total basin area, it contributed an average annual water yield volume of 11.29×10^9 m^3. In contrast, the WRB, which accounted for 3.65% of the basin, characterized by the lowest average annual precipitation (373.52 mm), average annual AET (223.85 mm), and average water yield rate (15.79%), resulting in an average annual water yield volume of 5.46×10^9 m^3. Overall, the water yield demonstrated a distinct spatial gradient, with higher values in the southeast and lower values in the northwest (Fig. 3). Eastern sub-basins (such as the TRB and ELRB) outperformed western sub-basins (such as the WLRB and WRB) in terms of precipitation and water yield, highlighting significant regional disparities in water resource distribution.

Table 3 Precipitation, actual evapotranspiration (AET), and water yield of the LRB from 1993 to 2022

Basin	Area ($\times10^4$ km^2)	Percentage of area (%)	Average annual precipitation (mm)	Average annual AET (mm)	Average annual water yield (mm)	Average annual water yield volume ($\times10^9$ m^3)	Average water yield rate (%)
LRB	21.46	100.00	483.15	235.59	247.54	53.13	26.84

Note: LRB, Liaohe River Basin.

Table 4 Precipitation, AET, and water yield of the six sub-basins from 1993 to 2022

Sub-basin	Area ($\times10^4$ km^2)	Percentage of area (%)	Average annual precipitation (mm)	Average annual AET (mm)	Average annual water yield (mm)	Average annual water yield volume ($\times10^9$ m^3)	Average water yield rate (%)
ELRB	1.11	5.15	587.21	216.59	370.64	4.10	40.43
TRB	2.60	12.09	710.37	275.46	434.96	11.29	47.67
MLRB	4.81	22.41	573.69	244.29	329.42	15.84	36.02
WLRB	5.22	24.31	416.37	230.70	185.65	9.69	19.93
XRB	4.08	19.02	387.38	222.12	165.22	6.75	17.67
WRB	3.65	17.01	373.52	223.85	149.66	5.46	15.79

Note: ELRB, East Liao River Basin; TRB, Taizi River Basin; MLRB, Middle Liaohe River Basin; WLRB, West Liao River Basin; XRB, Xinkai River Basin; WRB, Wulijimuren River Basin.

3.1.3 Hotspot and coldspot analysis of water yield

From 1993 to 2022, the water yield in the LRB exhibited statistically significant spatial clustering patterns based on Getis-Ord G_i^* analysis (P<0.05; Fig. 4). In five representative years—1993, 2000, 2005, 2010, and 2022—hotspots were predominantly distributed in the southeastern part of the basin, whereas coldspots were concentrated in the northwest. In 2015, the distribution pattern of coldspots shifted, clustering mainly in the western part of the basin, while the eastern region displayed notable hot spots (Fig. 4e). Overall, from 1993 to 2022, coldspot clusters were primarily located in the northwestern WRB and WLRB sub-basins, while hotspots were significantly concentrated in the TRB, eastern MLRB, and ELRB sub-basins (Fig. 4g). These spatial distribution patterns highlighted pronounced regional disparities in water yield across the LRB, which can inform targeted strategies for water resource management and ecological conservation.

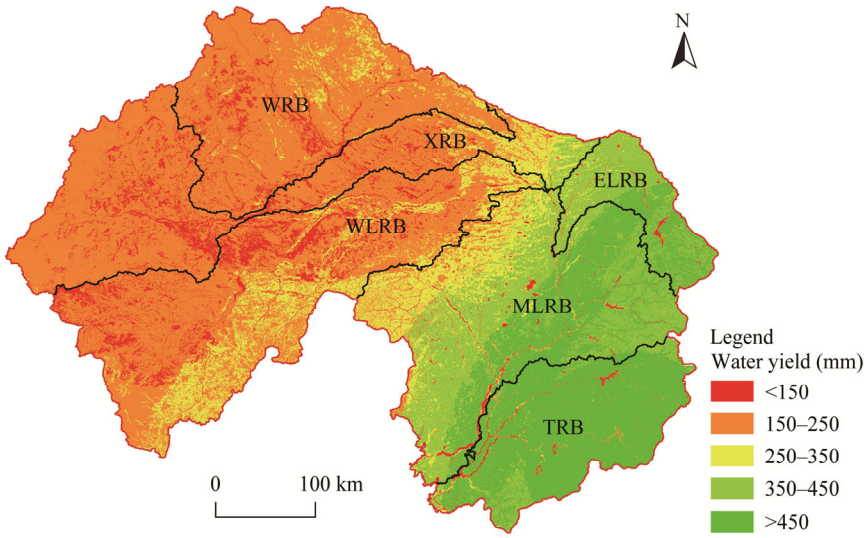

Fig. 3 Spatial variation of water yield in the LRB from 1993 to 2022

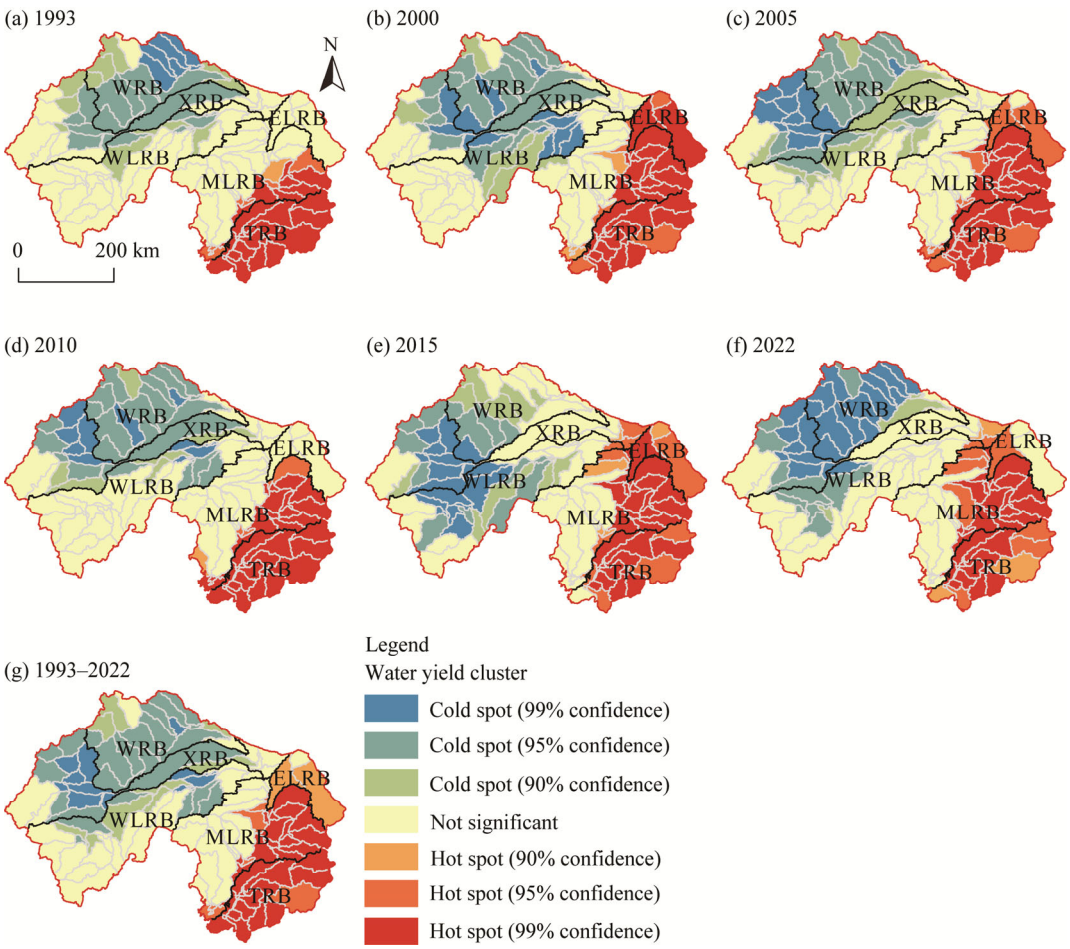

Fig. 4 Clustering characteristics of water yield in the LRB from 1993 to 2022. (a), 1993; (b), 2000; (c), 2005; (d), 2010; (e), 2015; (f), 2022; (g), 1993–2022.

3.2 Variations in water yield across different land use types

The water yield of different land use types in the LRB exhibited significant variation. Cultivated land had the highest average annual water yield (334.27 mm), followed by construction land (263.50 mm), forest land (246.99 mm), grassland (171.34 mm), and unused land (106.62 mm). In contrast, water body had the lowest water yield (0.95 mm). Notably, the combined contribution of artificial surfaces (cultivated land and construction land) accounted for 62.00% of the total water yield in the LRB, highlighting the significant impact of human activities on the basin's hydrological processes. Overall, cultivated land was the largest contributor to water yield, with construction land and forest land also making substantial contributions.

From 1993 to 2022, the average water yield rate of different land use types in the LRB varied significantly across sub-basins (Table 5). Among all land use types, cultivated land had the highest average water yield rate at 36.03%, followed by grassland (28.09%) and forest land (26.26%). Among the six sub-basins, TRB had the highest average water yield rate at 39.63%, followed by ELRB (30.66%) and MLRB (25.75%). In contrast, WRB had the lowest water yield rate at 11.67%. The average water yield rate of water bodies was negligible across all sub-basins. Overall, the TRB demonstrated the strongest water yield capacity across all land use types, while the WLRB, XRB, and WRB consistently showed lower average water yield rates.

Table 5 Water yield rate of different land use types in each sub-basin of the LRB from 1993 to 2022

Land use type	Average water yield rate (%)					
	ELRB	TRB	MLRB	WLRB	XRB	WRB
Cultivated land	43.97	54.51	41.83	26.85	25.87	23.10
Forest land	34.65	45.97	33.74	16.60	14.12	12.47
Grassland	38.89	50.73	26.54	19.44	17.05	15.89
Water body	0.00	0.01	0.00	0.00	0.00	0.00
Construction land	35.58	46.33	31.47	12.47	11.55	9.27
Unused land	30.88	40.23	20.90	9.41	10.78	9.29

3.3 Impact of climate change and land use change on water yield in the LRB

3.3.1 Impact of climate change on water yield

Precipitation varied notably among wet year, normal year, and dry year, averaging 564.34, 450.05, and 382.59 mm, respectively (Fig. 5). Compared with wet year, precipitation decreased 20.25% and 32.18% in normal year and dry year, respectively. Among all the six sub-basins, compared with wet year, the ELRB and MLRB experienced the largest reductions in precipitation in dry year, decreasing by 38.60% and 35.42%, respectively, followed by the WRB, which recorded a reduction of 33.89%. In contrast, AET exhibited relatively smaller variations under different climate scenarios. Across sub-basins, compared with wet year, the WRB and XRB underwent the most pronounced decreases in AET in dry year, with reductions of 15.06% and 12.40%, respectively.

Climate variability, primarily through changes in precipitation and AET, exerted a substantial influence on the distribution and spatial patterns of water yield in the LRB. The average water yield during wet year, normal year, and dry year was 318.54, 212.29, and 164.53 mm, respectively. Among the sub-basins, the ELRB and MLRM showed the highest sensitivity to changes in precipitation. Compared with wet year, water yield decreased 49.88% and 49.73% in normal year and dry year, respectively. The WRB exhibited the most significant change, with water yield decreasing by 57.90% under the same conditions.

3.3.2 Impact of land use change on water yield

From 1993 to 2022, land use change significantly affected water yield in the LRB (Fig. 6; Table 6). In the WRB and the XRB, large areas of forest land and grassland were converted to cultivated

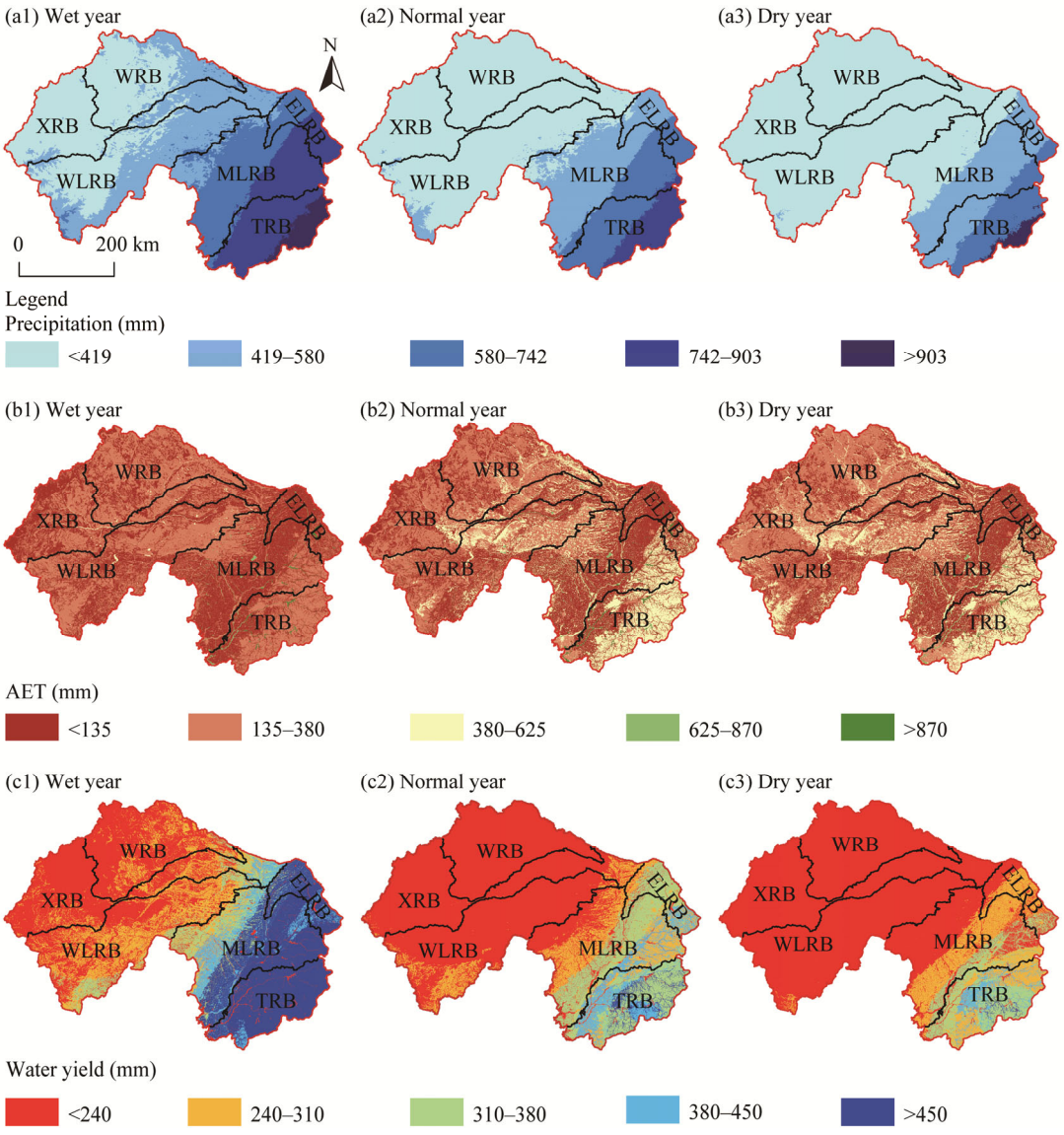

Fig. 5 Spatial distribution of precipitation (a1–a3), AET (b1–b3), and water yield (c1–c3) across wet year, normal year, and dry year in the LRB

land, with the area of cultivated land increasing by 512.81 and 981.22 km^2, respectively, leading to water yield volume increases of 1.19×10^9 and 2.32×10^9 m^3 (Table 7). In contrast, in the TRB, cultivated land was primarily converted to construction land and water body, with areas increasing by 1102.85 and 118.83 km^2, respectively, resulting in a water yield volume decrease of 4.58×10^9 m^3. Forest land expanded in most sub-basins, with the LRB, WRB, and XRB gaining 349.39, 91.64, and 79.95 km^2, respectively, which contributed to water yield volume increase of 0.48×10^9, 0.14×10^9, and 0.21×10^9 m^3. Grassland saw substantial declines, particularly in the MLRB and XRB, with reduction of 993.91 and 1015.84 km^2, causing water yield volume decrease of 2.98×10^9 and 1.82×10^9 m^3. Conversely, the WRB experienced a grassland increase of 605.79 km^2, resulting in a water yield volume increase of 0.95×10^9 m^3. Construction land expanded significantly, especially in the TRB, with an increase of 1102.85 km^2, resulting in water yield volume increase of 5.26×10^9 m^3, which is the largest contribution to water yield increase among all sub-basins. Unused land decreased sharply in the WRB, with a reduction of 1292.31 km^2, causing a water yield volume loss of 1.13×10^9 m^3, while in the MLRB, a slight increase of

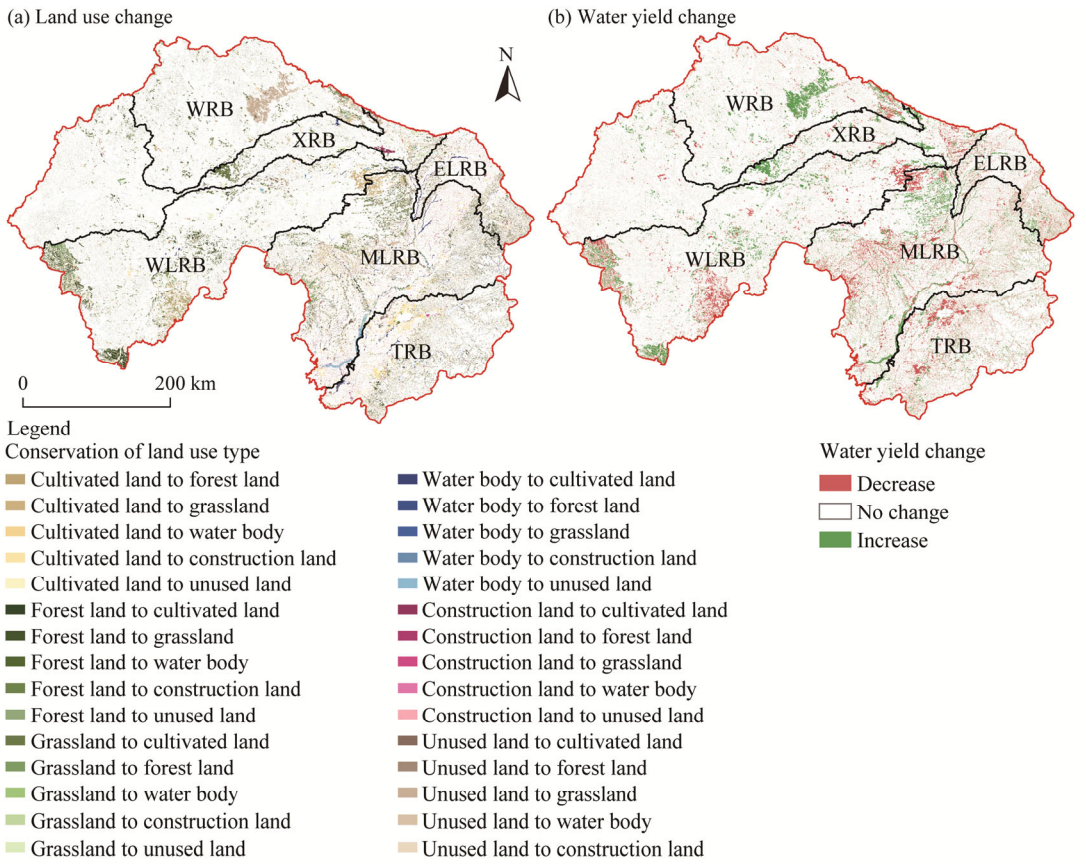

Fig. 6 Land use change (a) and corresponding change in water yield (b) of the LRB from 1993 to 2022

Table 6 Land use change of each sub-basin in the LRB from 1993 to 2022

Land use type	Area change (km^2)					
	ELRB	TRB	MLRB	WLRB	XRB	WRB
Cultivated land	58.03	–831.99	26.03	270.01	981.22	512.81
Forest land	70.70	–192.00	349.39	–111.14	79.95	91.64
Grassland	–121.08	–107.18	–993.91	–431.97	–1015.84	605.79
Water body	–97.38	118.83	–281.23	–50.48	–65.36	–0.78
Construction land	54.86	1102.85	473.65	218.51	–62.83	82.47
Unused land	33.85	–89.48	422.56	103.54	81.47	–1292.31

Table 7 Water yield change of each sub-basin in the LRB from 1993 to 2022

Land use type	Water yield change ($\times 10^9$ m^3)					
	ELRB	TRB	MLRB	WLRB	XRB	WRB
Cultivated land	0.28	–4.58	0.14	0.56	2.32	1.19
Forest land	0.17	–0.81	0.48	–0.37	0.21	0.14
Grassland	–0.47	–0.60	–2.98	–0.54	–1.82	0.95
Water body	0.00	0.00	0.00	0.00	0.00	0.00
Construction land	0.24	5.26	1.65	0.29	–0.11	0.07
Unused land	0.1	–0.31	1.45	0.12	0.21	–1.13

33.85 km^2 led to a water yield volume increase of 1.45×10^9 m^3. Changes in the area of water body were minimal and had negligible effects on water yield volume. Overall, cultivated land expansion and grassland degradation were the dominant drivers of water yield volume changes in the LRB, while forest land restoration and construction land expansion also contributed notable localized effects.

4 Discussion

4.1 Spatiotemporal patterns and variations of water yield

This study quantitatively assessed the water yield in the LRB using the InVEST model and explored its spatiotemporal variations from 1993 to 2022. The results indicated that the average annual precipitation in the LRB was 483.15 mm, exhibiting a significant upward trend with a growth rate of 27.03 mm/10a. Water yield also showed a slight but significant increasing trend, with a growth rate of 22.96 mm/10a. This suggested that the increase in precipitation has directly contributed to the rise in water yield. However, the relationship between precipitation and water yield is not linear, as it is mediated by factors such as AET and soil properties (Gharun et al., 2014). During the study period, AET exhibited a significant upward trend, with an increase rate of 4.07 mm/10a, indicating that rising temperatures may have enhanced atmospheric water demand, leading to increased evapotranspiration losses. This phenomenon aligns with the Budyko's framework, which describes the balance between water supply (precipitation) and demand (AET) in hydrological systems (Todhunter et al., 2020). Furthermore, the response of water yield in extreme years highlighted the sensitivity of the LRB to climate variability. For instance, in 2021, precipitation reached a peak of 667.00 mm, coinciding with the highest water yield of 408.90 mm, likely due to precipitation exceeding soil infiltration capacity, which promoted surface runoff and groundwater recharge. In contrast, in 2009, precipitation dropped to its lowest level of 353.00 mm, resulting in insufficient soil moisture and a minimum water yield of 145.10 mm.

Regarding spatial variation, the LRB exhibited significant heterogeneity in water yield, with eastern sub-basins (e.g., TRB and ELRB) showing notably higher water yield compared with western sub-basins (e.g., XRB and WRB). This spatial differentiation is primarily attributed to the east-west precipitation gradient, as the eastern regions, being closer to moisture sources, receive higher precipitation. However, local factors such as soil type and vegetation cover also play a critical role in regulating the spatial distribution of water yield. The soils in the eastern sub-basins have higher water retention capacity, facilitating runoff generation, while the more permeable soils in the western sub-basins promote deep percolation rather than surface water yield. This spatial pattern is consistent with findings from other arid and semi-arid regions, indicating that soil properties are key modulators of hydrological responses (Zhang et al., 2024). Using the hot-cold spot analysis method, the study further revealed distinct spatial clustering characteristics, with hotspots mainly concentrated in the eastern part of the basin and coldspots in the western part. To address this spatial heterogeneity, it is recommended to implement ecological conservation measures, such as vegetation restoration and rainwater harvesting systems, in water yield hotspot regions to enhance water retention capacity and mitigate flood risks. In contrast, water yield coldspot regions should focus on improving irrigation efficiency, adopt water-saving technologies, and implement groundwater recharge projects (Chu et al., 2024). Such spatially differentiated water resource management strategies are essential for addressing regional hydrological challenges under climate change.

4.2 Impact of changes in climate and land use on water yield

The results of this study indicated that both climate change and land use change had significant impacts on the spatiotemporal variation of water yield in the LRB. The study showed that precipitation had a much stronger effect on water yield than evapotranspiration. The variation in

precipitation directly influenced water yield, with a more pronounced decrease in water yield as precipitation declined, particularly in dry years. Jiang et al. (2016) and Li et al. (2021b) also emphasized the dominant role of precipitation as the primary factor influencing water yield changes. Previous studies also suggested that climate change contributed over 90.00% to the changes in water yield (Hu et al., 2020), further supporting the central role of precipitation in water yield variations (Zhao et al., 2024). In addition, the steady increase in AET over the period from 1993 to 2022 (at a rate of 4.07 mm/10a) may have accelerated the hydrological cycle, influencing the spatial and temporal distribution of hydrological elements (Gusev et al., 2019; Cheng and Li, 2020).

Changes in land use, particularly the conversion among cultivated land, grassland, and construction land, significantly influenced water yield and other ecosystem services (Latinopoulos et al., 2021; Liang et al., 2021; Singkran et al., 2021). The study found that grassland has a lower water yield compared with cultivated land, construction land, and forest land, which is consistent with the findings of Hu et al. (2022) in the Yangtze River Basin. Nevertheless, grassland offers significant advantages in regulating the hydrological cycle, reducing runoff, and conserving soil and water, making it the optimal land use type for maintaining hydrological balance (Li et al., 2021b). For example, in the WRB, water yield increased after land use shifted from other types to grassland, consistent with the advantages of grassland in regulating water cycles (Fig. 6). However, the negative impact of LUCC on water yield was also significant. In particular, the expansion of construction land in the TRB led to a decrease in water yield. The increase in construction land altered subsurface conditions by converting vegetated surfaces into impervious layers, reducing evapotranspiration, and increasing the demand for water resources, which in turn affected the distribution of water yield within the basin (Anache et al., 2018). These changes highlighted the complex impact of human activities on water yield, especially the increased pressure on water resources due to urbanization and the expansion of construction land.

Both climate change and land use change had profound impacts on the spatiotemporal distribution of water yield in the LRB from 1993 to 2022. Under different hydrological conditions (wet, normal, and dry years), variations in precipitation significantly influenced water yield. When precipitation decreased by 8.98%–38.60%, water yield reduced by 10.81%–49.88%. Water yield variations ranged from 5.17%–36.73%, corresponding to land use area changes of 4.91%–35.90%. These results indicated that precipitation, as a key factor of climate change, influenced the inter-annual variability and total magnitude of water yield, while land use change further shaped the spatial distribution of water yield by altering surface cover and ecosystem functions. Overall, climate variability—particularly changes in precipitation—played a dominant role in driving water yield changes in the LRB from 1993 to 2022, while land use change contributed to spatial heterogeneity (Nahib et al., 2021; Bejagam et al., 2022)

4.3 Research shortcomings and prospects

This study simulated the water yield of the LRB using the InVEST model, revealing its spatial and temporal distribution patterns. However, due to the model's simplification of the runoff process and its reliance solely on natural data inputs, without considering complex topography and geomorphology or social factors, uncertainties existed in the model itself (Wan et al., 2023). In addition, the input data for the water yield module, such as the vegetation evapotranspiration, the depth of root-restricting layer, and the soil content of silt, clay, and sand, were sourced from the World Soil Database, literature data, and FAO, while these datasets provided valuable information for simulating water yield, their accuracy varied depending on the regional characteristics and scale, which may have limited the overall precision of the model outputs (Yang et al., 2020). Moreover, as the LRB spanned a large area, there were considerable differences in soil conditions, precipitation, and evapotranspiration. The surface environment also

changed over time and space, making it challenging to ensure parameter accuracy. Furthermore, this study primarily explored the impact of climate change and land use change on water yield across the entire basin, but the combined effects of these factors on water yield had not been fully examined. Future research could simulate the synergetic effects of climate change and land use change to comprehensively assess their combined impacts on water yield.

5 Conclusions

This study used the InVEST model to analyze the spatiotemporal distribution patterns of water yield in the LRB from 1993 to 2022, investigating the response of water yield to climate change and land use change. From 1993 to 2022, the average annual precipitation in the LRB was 483.15 mm, with an average annual water yield of 247.54 mm, showing a slight upward trend. Water yield exhibited a distinct spatial pattern, with higher values in the southeast and lower values in the northwest. Significant differences in water yield were observed among the sub-basins, with the TRB having the highest water yield and the WRB having the lowest. Additionally, water yield demonstrated clear spatial clustering effects across the basin. Compared with AET, precipitation was the dominant climatic factor influencing water yield in the LRB. Cultivated land contributed the most to water yield, followed by construction land. Land use change had a significant impact on the spatial distribution of water yield, with the expansion of cultivated land and the reduction of grassland being the primary drivers of changes in water yield. The combined impacts of climate change and land use change underscored the need to optimize water resource allocation and promote ecological conservation, in order to achieve sustainable and efficient water resource use.

Conflict of interest

The authors declare that they have no known competing financial interests or personal relationships that could have appeared to influence the work reported in this paper.

Acknowledgements

This work was funded by the Liaoning Provincial Social Science Planning Fund (L22AYJ010).

Author contributions

Conceptualization: LYU Leting; Data curation: JIANG Ruifeng; Methodology: LYU Leting, JIANG Ruifeng; Investigation: JIANG Ruifeng; Formal analysis: LYU Leting; Writing - original draft preparation: JIANG Ruifeng; Writing - review and editing: JIANG Ruifeng; Funding acquisition: LYU Leting, ZHENG Defeng; Resources: LYU Leting, ZHENG Defeng; Supervision: ZHENG Defeng; Project administration: LYU Leting; Software: LIANG Liheng; Validation: LYU Leting, LIANG Liheng; Visualization: LIANG Liheng. All authors approved the manuscript.

References

Anache J A A, Flanagan D C, Srivastava A, et al. 2018. Land use and climate change impacts on runoff and soil erosion at the

hillslope scale in the Brazilian Cerrado. Science of the Total Environment, 622–623: 140–151.

Bejagam V, Keesara V R, Sridhar V. 2022. Impacts of climate change on water provisional services in Tungabhadra Basin using InVEST model. River Research and Applications, 38(1): 94–106.

Cheng B, Li H E. 2020. Impact of climate change and human activities on economic values produced by ecosystem service functions of rivers in water shortage area of Northwest China. Environmental Science and Pollution Research, 27: 26570–26578.

Chu J Y, Wang Z C, Bao X G, et al. 2024. Addressing the contradiction between water supply and demand: a study on multi-objective regional water resources optimization allocation. Environment, Development and Sustainability, doi: 10.1007/s10668-024-05214-z.

Daneshi A, Brouwer R, Najafinejad A, et al. 2021. Modelling the impacts of climate and land use change on water security in a semi-arid forested watershed using InVEST. Journal of Hydrology, 593: 125621, doi: 10.1016/j.jhydrol.2020.125621.

Dashtbozorgi F, Hedayatiaghmashhadi A, Dashtbozorgi A, et al. 2023. Ecosystem services valuation using InVEST modeling: Case from southern Iranian mangrove forests. Regional Studies in Marine Science, 60: 102813, doi: 10.1016/j.rsma.2023.102813.

Donohue R J, Roderick M L, McVicar T R. 2012. Roots, storms and soil pores: Incorporating key ecohydrological processes into Budyko's hydrological model. Journal of Hydrology, 436–437: 35–50.

Emlaei Z, Pourebrahim S, Heidari H, et al. 2022. The impact of climate change as well as land-use and land-cover changes on water yield services in Haraz Basin. Sustainability, 14(13): 7578, doi: 10.3390/su14137578.

Getis A, Ord J K. 1995. Local spatial autocorrelation statistics: distributional issues and an application. Geographical Analysis, 27(4), 286–306.

Gharun M, Vervoort R W, Turnbull T L, et al. 2014. A test of how coupling of vegetation to the atmosphere and climate spatial variation affects water yield modelling in mountainous catchments. Journal of Hydrology, 514: 202–213.

Gomariz-Castillo F, Alonso-Sarría F, Cabezas-Calvo-Rubio F. 2018. Calibration and spatial modelling of daily ET_0 in semiarid areas using Hargreaves equation. Earth Science Informatics, 11: 325–340.

Griffith D A. 2021. Interpreting Moran eigenvector maps with the Getis-Ord Gi* statistic. The Professional Geographer, 73(3): 447–463.

Guo Q, Yu C X, Xu Z H, et al. 2023. Impacts of climate and land-use changes on water yields: Similarities and differences among typical watersheds distributed throughout China. Journal of Hydrology: Regional Studies, 45: 101294, doi: 10.1016/j.ejrh.2022.101294.

Gusev E M, Nasonova O N, Kovalev E E, et al. 2019. Impact of possible climate change on extreme annual runoff from river basins located in different regions of the globe. Water Resources, 46(Suppl. 1): S126–S136.

Hasan S S, Lin Z, Miah M G, et al. 2020. Impact of land use change on ecosystem services: A review. Environmental Development, 34: 100527, doi: 10.1016/j.envdev.2020.100527.

Hu W M, Yang R H, Jia G Y, et al. 2022. Response of water yield function to land use changes and its driving factors in the Yangtze River Basin. Acta Ecologica Sinica, 42(17): 7011–7027. (in Chinese)

Hu Y F, Gao M, Batunacun. 2020. Evaluations of water yield and soil erosion in the Shaanxi-Gansu Loess Plateau under different land use and climate change scenarios. Environmental Development, 34: 100488, doi: 10.1016/j.envdev.2019.100488.

Jiang C, Li D Q, Wang D W, et al. 2016. Quantification and assessment of changes in ecosystem service in the Three-River Headwaters Region, China as a result of climate variability and land cover change. Ecological Indicators, 66: 199–211.

Jiang D, Xin Y D. 2022. Study on the impact of meteorological factors on evapotranspiration in the Liaohe River Basin. Water Resources & Hydropower of Northeast China, 40(11): 33–34. (in Chinese)

Kiziloglu F M, Sahin U, Kuslu Y, et al. 2009. Determining water–yield relationship, water use efficiency, crop and pan coefficients for silage maize in a semiarid region. Irrigation Science, 27: 129–137.

Latinopoulos D, Koulouri M, Kagalou I. 2021. How historical land use/land cover changes affected ecosystem services in Lake Pamvotis, Greece. Human and Ecological Risk Assessment, 27(6): 1472–1491.

Li M, Li S S, Liu H C, et al. 2023. Balancing water ecosystem services: assessing water yield and purification in Shanxi. Water, 15(18): 3261, doi: 10.3390/w15183261.

Li M Y, Liang D, Xia J, et al. 2021a. Evaluation of water conservation function of Danjiang River Basin in Qinling Mountains, China based on InVEST model. Journal of Environmental Management, 286: 112212, doi: 10.1016/j.jenvman.2021.112212.

Li R J, Li H M, Wu F F, et al. 2024a. Study on the spatial differentiation pattern and driving forces of ecosystem services in

Qinghai Lake Basin. Ecology and Environment Sciences, 33(2): 301–309. (in Chinese)

Li S, Du T, Gippel C J. 2022. A modified Fu (1981) equation with a time-varying parameter that improves estimates of inter-annual variability in catchment water balance. Water Resources Management, 36: 1645–1659.

Li X L, Xu X F, Sonnenborg T O, et al. 2024b. Effect of ecological restoration on evapotranspiration and water yield in the agro-pastoral ecotone in northern China during 2000–2018. Journal of Hydrology, 638: 131531, doi: 10.1016/j.jhydrol.2024.131531.

Li X Y, Guo J M, Qi S Z. 2021b. Forestland landscape change induced spatiotemporal dynamics of subtropical urban forest ecosystem services value in forested region of China: A case of Hangzhou City. Environmental Research, 193: 110618, doi: 10.1016/j.envres.2020.110618.

Liang J, Li S, Li X D, et al. 2021. Trade-off analyses and optimization of water-related ecosystem services (WRESs) based on land use change in a typical agricultural watershed, southern China. Journal of Cleaner Production, 279: 123851, doi: 10.1016/j.jclepro.2020.123851.

Malhi Y, Franklin J, Seddon N, et al. 2020. Climate change and ecosystems: threats, opportunities and solutions. Philosophical Transactions of the Royal Society B, 375(1794): 20190104, doi: 10.1098/rstb.2019.0104.

Mao C R, Dai L M, Qi L, et al. 2020. Constructing of ecological security pattern based on ecosystem services: A case study of the Liaohe River Basin, Liaoning Province, China. Acta Ecologica Sinica, 40(18): 6486–6494. (in Chinese)

Nahib I, Ambarwulan W, Rahadiati A, et al. 2021. Assessment of the impacts of climate and LULC changes on the water yield in the Citarum River Basin, West Java Province, Indonesia. Sustainability, 13(7): 3919, doi: 10.3390/su13073919.

Ningrum A, Setiawan Y, Tarigan S D. 2022. Annual water yield analysis with InVEST model in Tesso Nilo National Park, Riau Province. IOP Conference Series: Earth and Environmental Science, 950: 012098, doi: 10.1088/1755-1315/950/1/012098.

Qi X K, Li Q, Yue Y M, et al. 2021. Rural–urban migration and conservation drive the ecosystem services improvement in China karst: A case study of Huanjiang County, Guangxi. Remote Sensing, 13(4): 566, doi: 10.3390/rs13040566.

Redhead J W, Stratford C, Sharps K, et al. 2016. Empirical validation of the InVEST water yield ecosystem service model at a national scale. Science of the Total Environment, 569–570: 1418–1426.

Ren Q R, Liu D D, Liu Y F. 2023. Spatio-temporal variation of ecosystem services and the response to urbanization: Evidence based on Shandong Province of China. Ecological Indicators, 151: 110333, doi: 10.1016/j.ecolind.2023.110333.

Rodríguez V A, Mazza S M. 2020. The impact of land use change on water resources. International Water and Irrigation, doi: 10.52783/iwi.v39i2.20.

Singkran N, Intharawichian N, Anantawong P. 2021. Determining land use influences on the hydrologic regime of the Chao Phraya River Basin, Thailand. Physics and Chemistry of the Earth, Parts A/B/C, 121: 102978, doi: 10.1016/j.pce.2021.102978.

Song S, Fang L H, Yang J X, et al. 2024. The spatial-temporal matching characteristics of water resources and socio-economic development factors: A case study of Guangdong Province. Water, 16(2): 362, doi: 10.3390/w16020362.

Todhunter P E, Jackson C C, Mahmood T H, et al. 2020. Streamflow partitioning using the Budyko framework in a northern glaciated watershed under drought to deluge conditions. Journal of Hydrology, 591: 125569, doi: 10.1016/J.HYDROL.2020.125569.

Wan Z G, Ding W G, Pu X T, et al. 2023. Analysis of temporal and spatial changes in water yield and driving factors in Qilian Mountain National Park. Journal of Soil and Water Conservation, 37(6): 161–169. (in Chinese)

Wang X J, Liu G X, Lin D R, et al. 2022a. Water yield service influenced by climate and land use change based on InVEST model in the monsoon hilly watershed in South China. Geomatics, Natural Hazards and Risk, 13(1): 2024–2048.

Wang Y F, Ye A Z, Peng D Z, et al. 2022b. Spatiotemporal variations in water conservation function of the Tibetan Plateau under climate change based on InVEST model. Journal of Hydrology: Regional Studies, 41: 101064, doi: 10.1016/j.ejrh.2022.101064.

Wu C X, Qiu D X, Gao P, et al. 2022. Application of the InVEST model for assessing water yield and its response to precipitation and land use in the Weihe River Basin, China. Journal of Arid Land, 14(4): 426–440.

Xu Z X, Liu X C, Li Y L. 2015. Zoning of aquatic ecoregions at levels I and II: Case study in Liaohe Basin. Advances in Science and Technology of Water Resources, 35(5): 176–180. (in Chinese)

Yang J, Xie B P, Zhang D G, et al. 2020. Response of temporal and spatial changes in water yield in the Yellow River Basin to precipitation and land use changes based on the InVEST model. Chinese Journal of Applied Ecology, 31(8): 2731–2739. (in Chinese)

Yang Y. 2024. Evaluation of water security in Liaohe River Basin. Heilongjiang Hydraulic Science and Technology, 52(1):

155–159. (in Chinese)

Yin L C, Feng X M, Fu B J, et al. 2021. A coupled human-natural system analysis of water yield in the Yellow River Basin, China. Science of the Total Environment, 762: 143141, doi: 10.1016/j.scitotenv.2020.143141.

Yudistiro, Kusratmoko E, Semedi J M. 2019. Water availability in Patuha Mountain region using InVEST model "hydropower water yield". E3S Web of Conferences, 125: 01015, doi: 10.1051/e3sconf/201912501015.

Zhang K W, Zhang Q, Wang G, et al. 2024. Spatiotemporal interactions between soil moisture and water availability across the Yellow River Basin, China. Journal of Hydrology: Regional Studies, 54: 101874, doi: 10.1016/j.ejrh.2024.101874.

Zhang S D. 2021. Study on the relationship between supply and demand of ecosystem services in Liaohe River Basin. MSc Thesis. Yanji: Yanbian University. (in Chinese)

Zhang S D, Li M Y, Xiang H X, et al. 2021a. Trade-offs and synergies of ecosystem services in the Liaohe River Basin. Agricultural Science Journal of Yanbian University, 43(1): 73–83. (in Chinese)

Zhang Y C, Rossow W B, Lacis A A, et al. 2004. Calculation of radiative fluxes from the surface to top of atmosphere based on ISCCP and other global data sets: Refinements of the radiative transfer model and the input data. Journal of Geophysical Research Atmospheres, 109(D19): D19105, doi: 10.1029/2003JD004457.

Zhang Y L, Guo X L, Wang N, et al. 2021b. Analysis on the optimal sowing date of dry-land winter wheat under different precipitation pattern based on wheat decision system. Chinese Journal of Agrometeorology, 42(6): 475–485. (in Chinese)

Zhang Z D, Yang Y, Chen Y C, et al. 2020. Spatial-temporal analysis of water supply services at different scales in the Wuhua River Basin. Geoinformatics in Sustainable Ecosystem and Society, 1228: 290–306.

Zhao Y Z, Wang L C, Jiang Q X, et al. 2024. Sensitivity of gross primary production to precipitation and the driving factors in China's agricultural ecosystems. Science of the Total Environment, 948: 174938, doi: 10.1016/j.scitotenv.2024.174938.

Zheng C X. 2018. Study on matching degree of water resources status and social economic development in Liaohe River Basin. Water Resources Planning and Design, 6: 1–3, 41. (in Chinese)